THE PHYSICS OF LASER-PLASMA INTERACTION IN GASEOUS TARGETS*

Eli Yablonovitch

Gordon McKay Laboratory

Harvard University

ABSTRACT

In studying the fundamental physics of laser-plasma interaction, gaseous targets offer some definite advantages over solid targets. Because they are experimentally cleaner and more controllable, gaseous targets have enabled us to isolate some specific physical processes. For example, we have found fast electron emission in a direction 30° away from the electric vector of the light wave, but in the plane of optical polarization. This effect is the clear signature of the resonant acceleration mechanism for laser beam absorption. The angle of electron emission determines the plasma density scale length. In addition, we have used the sudden plasma nucleation in a gas target as an optical shutter. This has resulted in the generation of 30 psec CO_2 laser pulses--a record. There will also be some discussion of the possibility of compressing a gaseous target to produce net fusion energy.

I. INTRODUCTION

This paper will be different in one very important respect from most of the other experimental papers in this volume. Most experiments in laser-plasma interaction are performed at the interface of a solid target, while those to be described here, occur in initially homogeneous gas target. The plasma is created inside a gas cell, at the focus of a lens.

We will show that gaseous targets can be very helpful in doing controlled experiments on the basic physics [1] of laser-plasma

interaction. Broadly speaking, the same physical phenomena are present as in solid target experiments. The small differences that do occur, tend to illuminate our physical understanding rather than obscure it.

We will divide the material of this paper into three sections. In the first we will describe the use of a gaseous target as a laser-plasma shutter. This type of shutter is the heart of the Optical Free Induction Decay (OFID) pulse generator. It has recently [2] produced 30 psec CO_2 laser pulses, a record for short duration with this type of laser. We will also describe the very important techniques for exceeding [3] the avalanche threshold for breakdown. The discovery [4] that the avalanche threshold intensity could be exceeded, even by 3 or 4 orders of magnitude, is the central fact that makes possible all further applications of gaseous targets. In connection with this, the methods of triggering and synchronizing [5] the plasma formation (or breakdown) will also be described.

In the second section we will discuss the mechanisms for the propagation of ionization fronts in gaseous targets. It will become apparent that the high speed motion of the ionization front is playing an important role in determining the speed of the plasma-shutter. The mechanism of propagation, decides whether there is compression behind the ionization front. This determines the plasma density, which is the crucial variable in laser-plasma interaction.

In the final section, we will describe a simple experiment which represents the first direct observation of the resonant acceleration effect in laser plasma interaction. This effect [6] is becoming more and more widely accepted [7] as being responsible for the efficient laser energy deposition in plasmas.

II. PICO-SECOND CO_2 LASER PULSES

The growth of plasma in an initially neutral medium occurs by avalanche ionization. Up until 1973 it was felt that the threshold intensity for plasma formation was essentially an avalanche threshold. The laser intensity had to be high enough to produce a sufficient number of e-foldings of the electron number (about e^{20}) during the available time. This can be expressed as

$$N = N_o \exp(gT)$$

where T is the pulse duration and N_o and N are the initial and final electron number respectively. The intensity dependence of the avalanche growth rate g is well known by scaling laws [8]

from the familiar dc avalanche ionization rates. When g becomes large enough, breakdown occurs.

This point of view was radically altered in 1973, when it was found [4] that under clean gas conditions there would be no free electrons available to initiate the avalanche. This was particularly evident at the CO_2 laser wavelength, for which the avalanche thresholds ($\sim 10^9 W/cm^2$) are relatively low. The avalanche threshold could be exceeded by 3 or 4 orders of magnitude before breakdown would occur [9,3]. This is the central experimental discovery which has permitted gaseous targets to be used in the many versatile ways to be discussed here.

At the very high intensities ($\sim 10^{13} W/cm^2$) g is very large, orders of magnitude larger than $1/T$. Therefore, when plasma nucleation finally does occur, the plasma density will grow with great speed and suddenness. The plasma becomes overdense in a very short time, blocking transmission of the laser beam through the gas. In actual practice the spatial growth is more important than the temporal growth in determining the speed of the "plasma-shutter." Figure 1 shows the transmission of light in the focal region of the gas. The fall time τ of the "plasma-shutter" is the time required for the ionization front to propagate across the focal spot.

$$\tau = L/V \qquad (1)$$

where L is the width of the focal spot and V is the speed of the ionization front. Measurements [9,2] have indicated that τ can be in the 10 picosecond range and V can be as high as 10^8 cm/sec, though improvements on these performance parameters will certainly occur in the future.

By now the reader will have noticed that the "plasma-shutter" has a fast fall time τ, but what is really wanted is a fast rise time. This, together with a variable pulse duration can be obtained by Optical Free Induction Decay (OFID) [10,11]. A physical description of OFID can be seen in Figure 2.

The output of the "plasma-shutter" is sent into an absorption cell containing hot CO_2. Although there is zero transmission through the absorption cell, the transmitted electric field may be regarded as the destructive interference of two non-zero quantities

$$E_{trans} = E_{in} + E_{mol} \equiv 0$$

where E_{mol}, the field generated by the vibrations of the CO_2 molecules exactly cancels E_{in} the laser field. Now if E_{in} suddenly goes to zero due to the action of the plasma shutter, the molecules

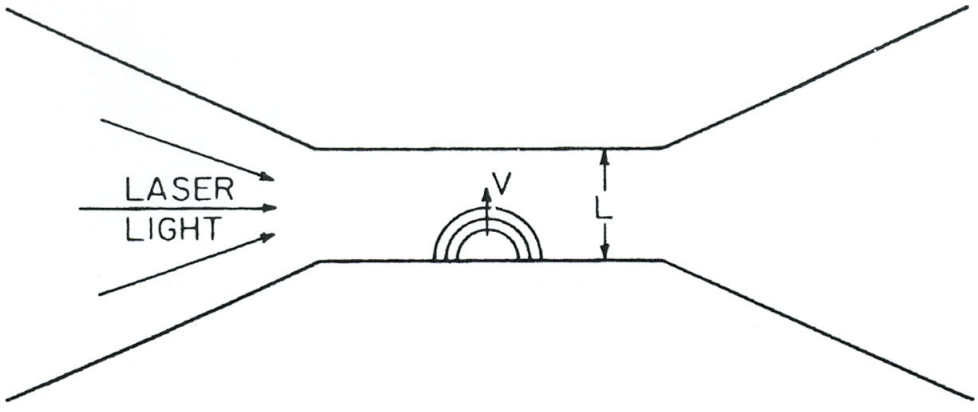

FIGURE 1. The ionized region spreads across the focal spot at a speed V, blocking transmission of the laser beam. The overdense plasma behaves like the blade of a light chopper, cutting across the optical path. This device is called the plasma shutter.

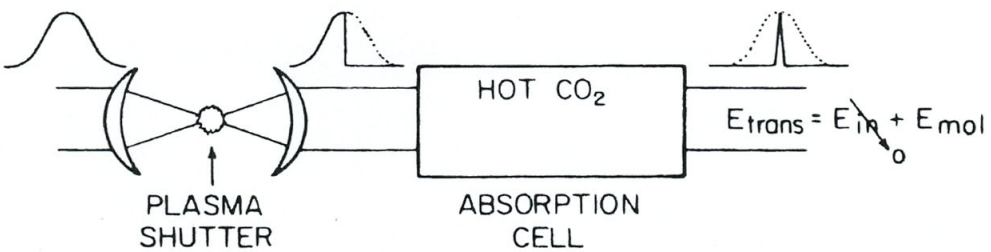

FIGURE 2. The optical field transmitted through the absorption cell, $E_{trans} = E_{in} + E_{mol}$ becomes non-zero when E_{in} is cut-off by the "plasma-shutter." The transmitted pulse is generated by free induction decay of the molecules and has a duration of the order of the molecular collision time.

continue to radiate E_{mol} for about a molecular relaxation time. E_{trans} becomes non-zero and equal to $E_{mol} = -E_{in}$ for about one collision time before the molecular field dies away.

$$E_{trans} = \cancel{E_{in}}_{\,o} + E_{mol} = -E_{in}$$

The OFID pulse is equal in amplitude to the input pulse E_{in}, opposite in phase, and has a duration of the order of the molecular collision time. This is readily controlled by varying the pressure in the hot CO_2 absorption cell.

The combination of plasma shutter and OFID cell has produced 30 picosecond CO_2 laser pulses. This duration has been determined by 2nd harmonic generation in GaAs and 2-photon correlation. The result of such a measurement [5] is shown in Fig. 3.

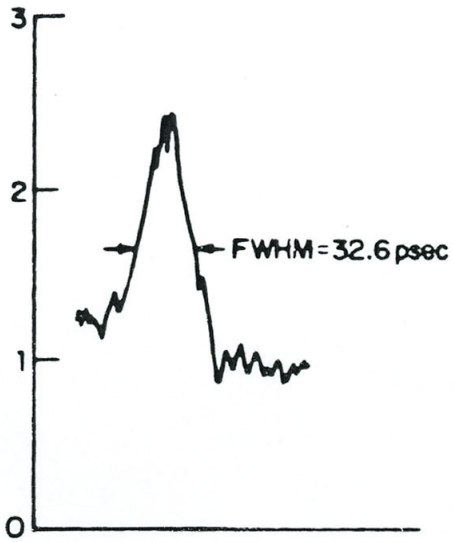

FIGURE 3. A 2-photon correlation scan of an ultra-short CO_2 pulse generated by OFID. The correlation was performed by 2nd harmonic generation in GaAs. For details see reference [2].

The short pulses have been amplified up to the 0.15 Joule level [12] for further laser-plasma interaction experiments. Due to limitations in the bandwidth [13] of the amplifier, which operated a 1 atm., the amplified pulses were no shorter than 500 psec. Ultra-short high energy laser pulses would require multi-atmosphere amplifiers.

OFID has now also been used to generate short pulses for the Iodine laser at 1.315 μ [14]. The pulse duration in that case seems also to be limited by the speed of the plasma shutter. More work is needed to determine whether the plasma shutter at the shorter wavelength can be equally fast as at 10.6 μ, the CO_2 wavelength.

An important aspect of the plasma shutter remains to be discussed. It had been mentioned that the avalanche ionization threshold can be greatly exceeded in a clean gas since there are no free electrons available to initiate the avalanche. If that is the case, then how does a plasma form at all? The answer is that in general, a plasma does not form, a breakdown does not occur! An initiating electron must somehow be introduced into the focal volume. One way of doing this, is by uv photo-ionization from a small pulsed electrical spark. The plasma formation is thereby externally synchronized with subnanosecond jitter [5]. Another method of synchronization is to split off ∿1% of the laser beam and focus it on a metal target. The uv photo-ionization triggers the breakdown in the main beam [15]. Finally if the intensity is high enough ($\sim 10^{13} W/cm^2$), then no external electron source is needed. The avalanche initiating electron will be produced by laser-induced tunnelling from the neutral molecules in the focal volume [3].

A final question has to do with the methods for cleaning up a gas to eliminate sources of free electrons. The simplest and best method is to employ the vapours of cryogenic liquids such as liquid nitrogen and helium. It is also helpful to use tight focusing to reduce the focal volume. Some success has also been attained by filtering bottled gas, but the intensity achievable in this way is not as great. It is important to recognize that the intensity of laser-plasma interaction in a gas target can never exceed the intensity at which the plasma first forms. Any further increase in intensity merely causes the ionization front to move upstream on the focused laser beam, with no intensity increase at the plasma front itself.

III. SPATIAL PROPAGATION OF THE IONIZATION FRONT

The velocity of motion of the ionization front plays a central role in the physics of gaseous targets. It determines the speed of the plasma shutter, the density of the plasma, its density gradient at the front and depending on the situation, the laser intensity at the front. It should be kept in mind that the motion of the ionization front into the neutral gas does not necessarily involve motion of the plasma particles themselves. Therefore the velocity of the front could be in the nature of a phase velocity, exceeding

the speed of light under some circumstances.

A good way to envision the motion of the ionization front is shown in Fig. 4. At a given instant in time near the front, let the plasma density n fall of exponentially with distance into the un-ionized gas, i.e., $n \sim n_o \exp\{-x/\mathscr{L}\}$ where $\mathscr{L}$ is the density scale height at the front. With the passage of time the plasma density at a fixed position grows at the avalanche growth rate g. Then $n \sim n_o \exp\{gt-x/\mathscr{L}\}$. Then iso-density contours move out at a speed $V = g\mathscr{L}$. The avalanche growth in time causes the ionization front to move out in space. A key role is played by the scale height $\mathscr{L}$, whose value is determined by one of a number of possible physical mechanisms.

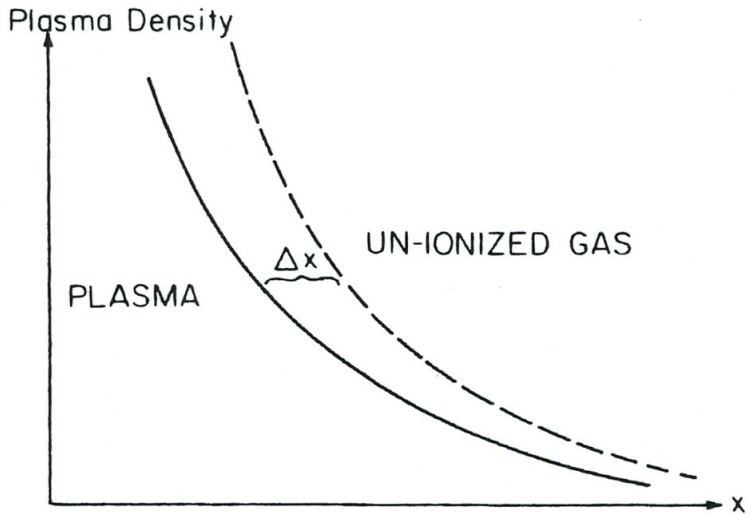

FIGURE 4. The plasma density at the ionization front falls off as $\exp\{-x/\mathscr{L}\}$ where $\mathscr{L}$ is the scale height (solid line). In a time t the density has grown $\exp\{gt\}$ by avalanche ionization (dashed line). The front has in effect moved forward a distance $\Delta x = g\mathscr{L}t$, making for a velocity $= g\mathscr{L}$.

The basic paper on the motion of laser-driven ionization fronts was written by Raizer [16] many years ago. He identified four basic mechanisms of propagation.

(a) Laser-driven shock front

(b) Laser Breakdown Wave

(c) Radiation driven ionization front

(d) Electron diffusion driven ionization front.

In practice the mechanism producing the fastest speed of motion will dominate. Mechanism (a), the laser driven shock wave states that the ionization front moves at the ion-sound speed relative to the plasma. This mechanism is always present, and may be regarded as setting a lower limit to the speed V. It involves a shock compression at the ionization front and therefore a density change accompanying passage of the front.

Mechanism (b) is applicable when the laser intensity is just equal to the avalanche breakdown field. It implicitly assumes that avalanche initiating electrons are present. Due to spatial inhomogeneities in the laser intensity distribution, different regions of space have different avalanche growth rates, causing the plasma formation to be delayed at the less intense points. If the scale length of the intensity distribution is L, then $\mathscr{L}$ the scale length of the plasma density, is somewhat less. (Since density depends exponentially on intensity.) Because the plasma density usually grows by $\exp\{20\}$, $\mathscr{L} \sim L/20$ is a good choice. The velocity of the front $V = gL/20$. Substituting this velocity into formula (1) the fall time of the plasma shutter becomes $\tau \approx 20/g$. The scaling laws [8] for g imply a value of ~ 20 picoseconds for τ, in agreement with measurements. For a faster fall time, there is definitely a premium in having g as large as possible at the instant of plasma nucleation. This may possibly be accomplished by operating the plasma shutter well in excess of atmospheric pressure, to increase the ionization rate.

The treatment given to mechanisms (c) and (d) by Raizer [16], implicitly assumed that the laser intensity was less than the breakdown field. Optical fields in excess of the avalanche threshold, were only discovered many years later. Therefore an analysis of mechanisms (c) and (d) in this high intensity regime is needed. Unfortunately there is insufficient space here to cover this material, but a paper for Phys. Fluids is being planned [17].

In mechanism (c) the plasma density distribution is set up by photo-ionization in the neutral gas. While in mechanism (d), the density distribution is set up by electron diffusion into the unionized gas. The important property of mechanisms (b), (c) and (d) is that they will generally result in a propagation velocity much greater than the ion sound speed of mechanism (a). Therefore, plasma rarefaction which occurs at the ion sound speed will be unable to keep up with the speed of the ionization front. Gas density will be unchanged upon passage of the front. The plasma density will be equal to the density of the gas in which it was formed.

There exists great interest [18] in producing a plasma whose density can be controlled to be at or near the critical density, $10^{19}/cm^3$, of the CO_2 laser, for the purpose of studying the laser plasma interaction. An experiment [1] of just this type will be described in the next section of this paper. At 150 torr H_2 gas the electron density is $10^{19}/cm^3$. Fig. 5 shows the fast electron emission caused by interactions at the critical density. Notice the sudden onset at 150 torr, confirming the idea that the ionization front is moving faster than the ion-sound speed. Measurements on the plasma shutter indicate that $V \sim 10^8$cm/sec while estimates of the electron temperature lead to ion sound speeds $\lesssim 2 \times 10^7$ cm/sec.

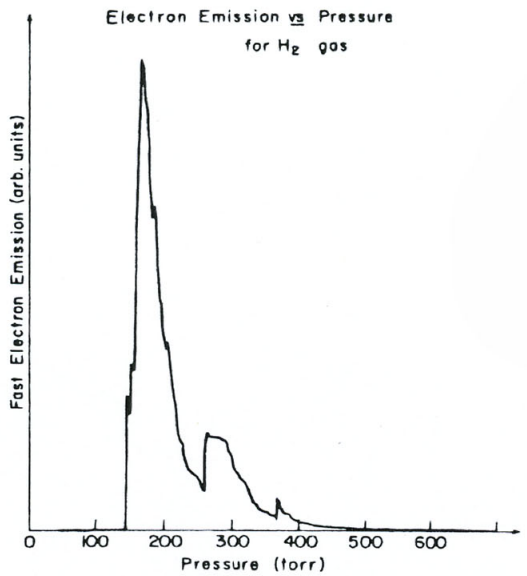

FIGURE 5. Notice the sudden onset of fast electron emission at 150 torr. At that pressure the gas density is 10^{19} atoms/c.c., the critical plasma density for the CO_2 laser. The output from a silicon radiation detector was averaged in a boxcar amplifier to produce this curve.

There has been some discussion recently [19] of the possibility of employing gaseous targets for laser fusion. If the ionization front moves at the ion sound speed as in mechanism (a) then the laser energy is converted to hydrodynamic work with rather high efficiency. If the speed is higher, as it would be under mechanisms (b), (c) and (d), then very little hydrodynamic work is accomplished. At the intensities which would be needed for laser fusion, $\gtrsim 10^{13}$ W/cm^2, it seems indeed that one of the unfavorable propagation mechanisms is likely to be at work [17]. If that is

the case, then gaseous targets would be inappropriate for fusion.

IV. RESONANCE ABSORPTION

The mechanism of light absorption remains one of the crucial unanswered questions in laser plasma interaction. Nevertheless, it is generally agreed that the energy is absorbed in the narrow critical layer where the plasma frequency ω_p equals the laser frequency ω. While many possible mechanisms have been proposed, the [20] parametric decay instability (PDI) and the resonant absorption (RA) effect [21] are most frequently mentioned.

In the PDI [20], the light wave drives an instability of electron plasma oscillations and ion sound waves propagating in the direction of the electric vector. As the plasma waves undergo Landau damping, they generate a superthermal tail of high energy electrons moving parallel and anti-parallel to the electric vector of the pump wave.

In the RA mechanism [22], the light is assumed obliquely incident on a varying plasma density profile. The light field penetrates the evanescent region and the electric vector component which is parallel to the plasma density gradient drives resonant oscillations at the critical layer. The plasma wave amplitude builds up until "wave breaking" or "electron overtaking" occurs [22]. Then the oscillatory energy of the electrons is converted to directed kinetic energy and they are ejected down (but not up) the plasma density. The effect is maximized at some oblique angle θ_m, whose exact value depends on the density-profile scale length L.

A good beginning toward understanding RA can be obtained from Fig. 6. A plasma with a fixed density gradient is placed between two capacitor plates driven at a frequency ω. The plasma density $n(x)$ varies from zero on one plate to overdense on the other plate. It passes through the critical density layer (dashed line) a distance L from the left hand plate. As is well-known from college physics, D, the electric displacement vector must be constant in such a capacitor. But the dielectric constant $\varepsilon(\omega)$ goes to zero at the critical layer, therefore the electric field E must diverge.

In practice, of course, the electric field must remain finite. This happens as follows: Let ξ represent the oscillatory displacement (Lagrangian coordinate) of a plasma electron about its starting position x. Since the equation of motion is a simple harmonic oscillator resonant at the plasma frequency $\omega_p(x)$:

$$\xi(x) = \frac{eE_o}{m} \frac{(-1)}{\left(\omega^2 - \omega_p^2(x) - \frac{i\omega}{\tau}\right)} \qquad (2)$$

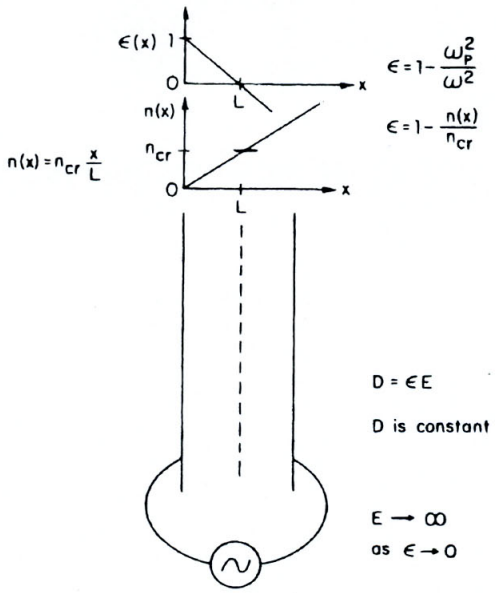

FIGURE 6. A parallel plate capacitor is filled with a plasma dielectric of varying density. The electric field E diverges in the critical density layer (dashed line) where $\varepsilon \to 0$. In practice, wave-breaking limits the electric field and accelerates some electrons down the density gradient.

This solution remains valid provided the electric field E_o is small enough [23] that the adjacent electron orbits do not overlap. If the electron orbits do intersect, the space charge of the adjacent electrons is neutralized. The Coulomb restoring force is reduced, the electrons are unable to complete their oscillatory cycle, but instead, are ejected from the plasma with the velocity they had at the instant of orbit overlap. The condition for orbit overlap, (also called "electron overtaking" or "wave-breaking") is given by:

$$\frac{d\xi}{dx} = -1$$

Applying this condition [24] to the simple harmonic formula (2), shows that the "wave-breaking" occurs during the phase of the motion when electrons are moving down the density gradient with a

kinetic energy:

$$\mathcal{E} = eE_o L \quad .$$

Therefore this resonant acceleration process ejects the electrons uni-directionally, i.e., down, but not up the density gradient.

The same conclusions apply for an electromagnetic wave incident on a plasma density gradient as shown in Fig. 7. Of course the wave must be obliquely incident as well as polarized in the plane of incidence in order to ensure an electric component parallel to the density gradient. As indicated in Fig. 7, total reflection occurs at $n_{cr} \cos^2\theta$ which is actually less than the critical density for non-normal incidence. Therefore the evanescent wave must tunnel through a forbidden region in order to reach the critical layer, as sketched in Fig. 8. At the critical layer, the normal component of E is resonantly enhanced, leading to wave-breaking and acceleration as before.

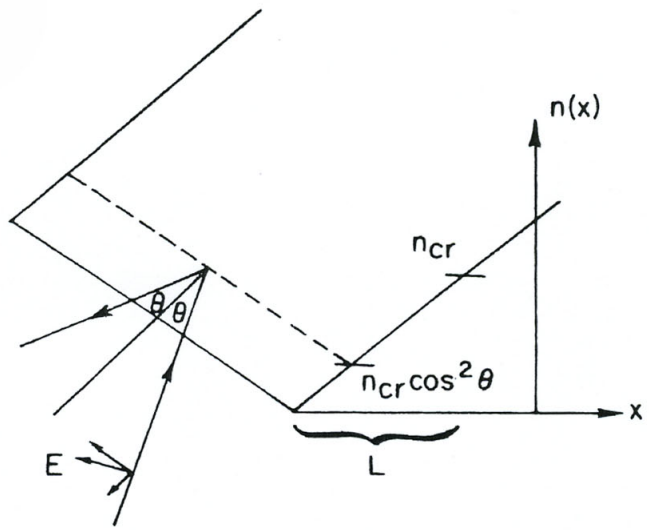

FIGURE 7. The geometry of resonant absorption. The em wave must be obliquely incident and polarized in the plane of incidence. Total reflection occurs at $n_{cr} \cos^2\theta$.

The optimum angle of incidence, θ_m, is determined by two competing physical effects. If θ is too small the normal component of E will vanish as $\sin\theta$. If θ is too large then the evanescent region is too thick and little light penetrates to the critical layer. The efficiency of tunnelling through the

evanescent region can be estimated by the WKB approximation.

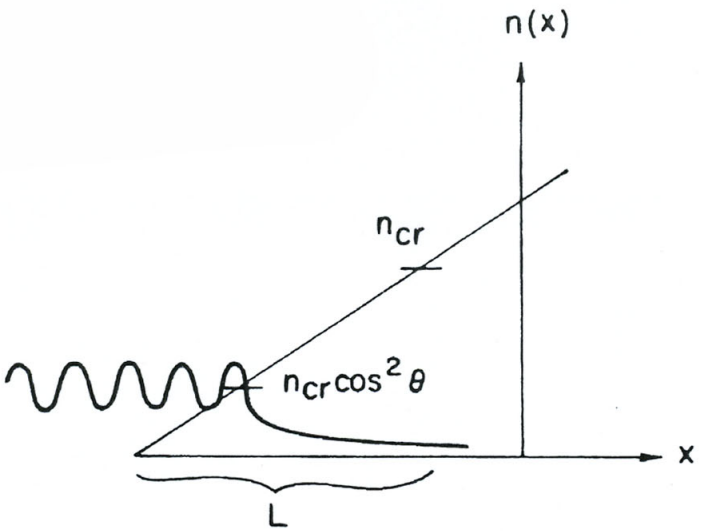

FIGURE 8. The evanescent wave must tunnel through a thickness $L(1-\cos^2\theta)$ before reaching the critical layer.

The two competing effects can then be combined into the following formula for the fraction of the incident electric field which is resonantly enhanced at the critical layer:

$$\sin\theta \quad \exp\left\{ - \int_{L\cos^2\theta}^{L} \sqrt{-k_x^2} \; dx \right\} \tag{3}$$

where

$$k_x^2 = k_o^2 \left(\cos^2\theta - \frac{x}{L} \right)$$

and k_o the vacuum propagation vector.

The optimum angle, θ_m, for resonant acceleration can be computed by differentiating formula (3) to obtain the condition for an extremum. The result is

$$2k_o L \sin^3\theta_m = 1$$

which differs from the exact numerically calculated [25] formula by a factor 1.5.

The basic experimental result is shown in Fig. 9:

(i) The electrons are emitted at an oblique angle with respect to the electric vector, in the plane formed by the electric vector and the propagation vector.

(ii) Furthermore, there are no electrons emitted anti-parallel to either of the two directions shown.

This is overwhelming evidence in favor of the RA mechanism.

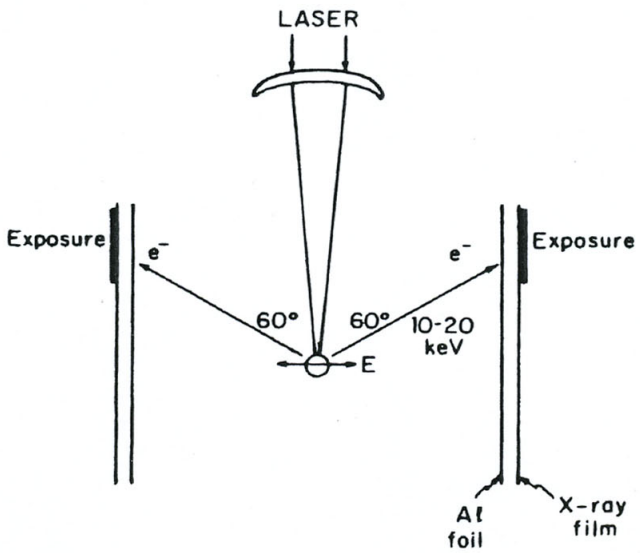

FIGURE 9. The laser is focused to produce a plasma in hydrogen gas. Fast electrons were emitted in the plane of the page, in the two directions shown. This proves that resonant absorption rather then the parametric decay instability is responsible for the acceleration.

The laser source was a Tachisto CO_2 single mode oscillator, followed by an optical free-induction-decay [11] (OFID) pulse shaper and a Lumonics 103 amplifier. This system is more fully described by Kwok and Yablonovitch [12]. The output is a diffraction limited pulse of 0.15 J energy and 500 psec duration. The beam was focused into a cell of hydrogen gas, by spherically corrected germanium lenses of aperture ratio varying from f/1 to f/5.

The gas was flowed, filtered and cold-trapped to remove impurities which might cause premature breakdown. For the same

reason, it was important to maintain a high peak to precursor contrast ratio in the laser pulse.

The electrons were detected by two means (i) a silicon surface barrier detector filtered by 3.5 mg/cm^2 of aluminum foil, and (ii) Kodak No-Screen medical X-ray film wrapped in a 3.5 mg/cm^2 thickness of Al foil. On the basis of the range-energy relations [16] in the H_2 gas, it was determined that the electrons had an energy of 10-20 keV. This was insufficient to penetrate the aluminum foil. Therefore they were detected indirectly, by means of the bremsstrahlung and Al K X-rays produced in the foil.

The film was bent into the shape of a cylinder of 4 cm diameter, co-axial with the laser beam in the center. Two typical exposures, made with an f/1 lens, are shown in Figs. 10(a) and (b). The two shots are similar in that the electrons are emitted

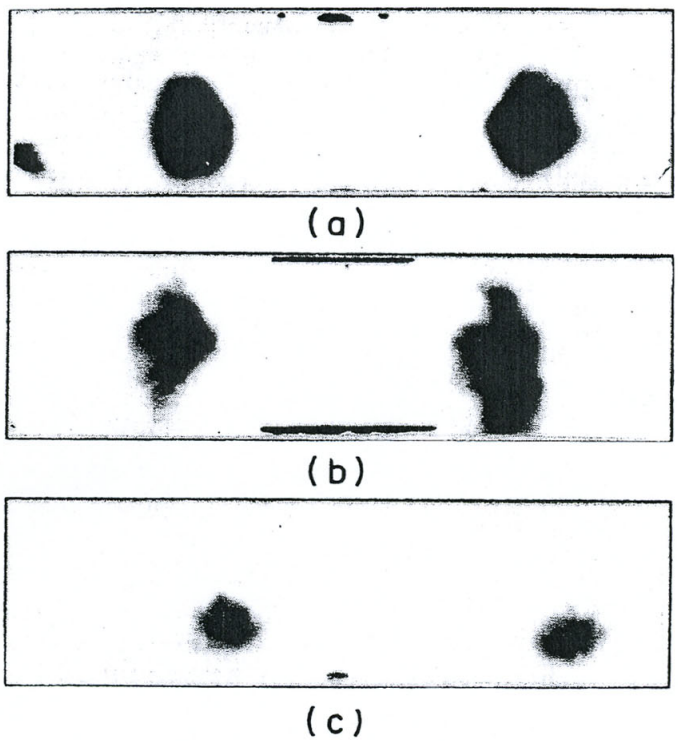

FIGURE 10. The X-ray film was bent in the shape of a cylinder, co-axial with the laser beam, and exposed to the fast electrons.
(a) and (b): Two typical shots. Notice the angular substructure in (b).
(c): The plane of polarization was rotated 45°. The two spots are correspondingly shifted.

on either side of the plasma, in the plane formed by the electric vector and the propagation vector. Nevertheless there are shot-to-shot fluctuations and differences. In particular Fig. 10(b) shows some substructure in the spots which represent the angular distribution of electrons.

As a double check, the plane of optical polarization was rotated by 45° using a germanium slab. The shifted spots in Fig 10(c) show that the directions of electron emission rotated an equivalent amount.

To determine more accurately the direction of electron emission relative to the light wave it was necessary to reduce the angular spread of propagation vectors by using a longer focal length lens. With an f/5 lens, the spread of k-vectors is only $\pm$ 5°, and Fig. 11 shows the result. Along the two edges of the film are the azimuthal and polar angles of electron emission with respect to the polarization and propagation vectors respectively. The electrons were emitted in the plane of optical polarization, but in a direction 30° backward from the electric vector. The half angle of the two cones of electron emission was about 25°. Therefore no electrons were accelerated into the forward half-sphere, i.e., into the anti-parallel directions.

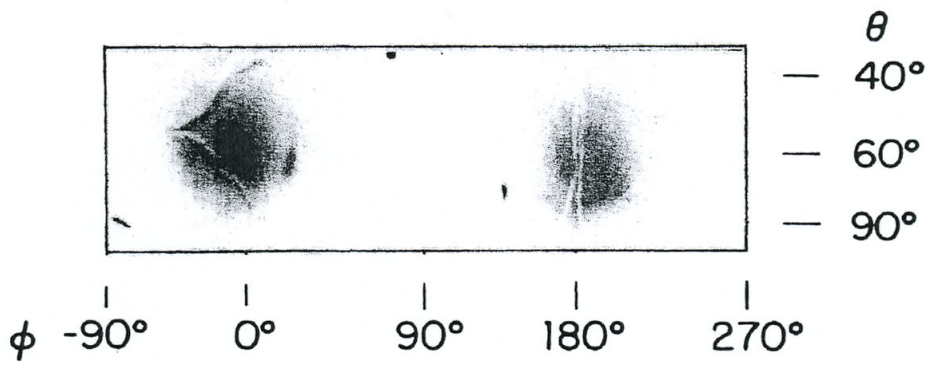

FIGURE 11. The exposure due to a plasma produced by an f/5 lens. In this case several hundred shots were needed. The thin white lines in the exposed regions are due to wrinkles in the Aluminum foil and they should be ignored. θ and ϕ are the spherical coordinates with respect to the propagation and polarization vector respectively.

The angle of incidence, θ_m, for maximum electron acceleration is usually given by the following formula which is valid for small θ_m:

$$3\, k_o L \sin^3 \theta_m = 1 \qquad (4)$$

where k_o is the vacuum propagation constant and L is the density profile scale length. From Fig. 4, $\theta_m = 60°$, which is somewhat too large for formula (4) to be really accurate. Nevertheless, we may conclude that $L \approx 1/2\ k$ or about one micron. Thus the angle of peak fast electron emission gives us information on the scale length L.

Armed with a knowledge of L, we are able to predict the energy of the fast electrons. A cold plasma "wave-breaking" analysis [24] is applicable under the physical conditions of our plasma. The "electron overtaking" condition [23] occurs at a kinetic energy $\mathscr{E} = eE_oL$. The evanescent electric field which penetrates to the critical layer, E_d, may be expressed in terms of the free space electric field, E_o by using the solution to Maxwell's equations given by Ginzburg [25].

$$E_d \approx \frac{E_o}{2\pi} \sqrt{\frac{\lambda}{L}}$$

Therefore, the electrons are ejected from the plasma with an energy

$$\mathscr{E} = \frac{eE_o\sqrt{\lambda L}}{2\pi} \quad .$$

For a laser intensity of 10^{14} W/cm^2 and $L \sim 1\mu$ (as inferred from θ_m) this yields an electron energy $\mathscr{E} \approx 15$ keV, well within the measured range of energies.

In general, fast electrons are emitted in all outward directions normal to the critical density surface. Nevertheless, the precise shape of this surface (spherical, ellipsoidal or irregular) plays only a minor role in the experiments reported here. This is because Equation (4) selects that angle θ_m along the surface for which the RA effect is maximized. The precise shape of the surface affects mainly the finite spread of angles about the maximum.

It should be kept in mind that the mechanism which produces the plasma density gradient in a gas target is inherently different from that in a solid target. In a gas the density gradient is determined by the propagation mechanism of the ionization front. The motion of the ions themselves is actually quite negligible. In a solid target on the other hand, the density profile is formed by ablation of ions from the surface. The motion of these ions is

strongly influenced by the ponderomotive pressure, and many types of filamentation instabilities [22] are rather probable.

This may explain why gas targets are more suitable for isolating the basic physical processes which occur in laser-plasma interaction. In a solid target there is always something additional taking place, and the simple angular emission described in Fig. 2 has apparently not been observed, though perhaps it soon will be.

More work is needed on the propagation mechanisms [16] of the laser-driven ionization front in a neutral gas. The measurement here, of the density profile scale length, $L \sim 1$ micron, is a good starting point. When combined with the avalanche growth rate g of the electron number density, we may deduce [17] a speed of propagation:

$$v = gL$$

The avalanche ionization scaling laws [8] imply a growth rate $g \approx 10^{12}$ sec^{-1} for H_2 at 150 torr, and 10^{14} W/cm^2. Therefore the calculated propagation speed is $v \approx 10^8$ cm/sec, in good agreement with measurements [4] on the speed [2] of the "plasma shutter."

REFERENCES

[1] Paul Kolodner and Eli Yablonovitch, Phys. Rev. Lett. 37, 1754 (1976).

[2] H. S. Kwok and Eli Yablonovitch, Appl. Phys. Lett. 30, Feb. 1, 1977.

[3] Jerry G. Black and Eli Yablonovitch, IEEE J. of Quant. Elec. JQE-13, April, (1976).

[4] Eli Yablonovitch, Phys. Rev. Lett. 31, 877 (1973).

[5] H. S. Kwok and Eli Yablonovitch, Appl. Phys. Lett. 27, 583 (1975).

[6] J. P. Friedberg, R. W. Mitchell, R. L. Morse and L. I. Rudsinski, Phys. Rev. Lett. 28, 795 (1972).

[7] H. G. Ahlstrom et al., J. Opt. Soc. Amer. to be published.

[8] Eli Yablonovitch, Appl. Phys. Lett. 23, 121 (1973).

[9] Eli Yablonovitch, Phys. Rev. A10, 1888 (1974).

[10] R. G. Brewer and R. L. Shoemaker, Phys. Rev. A6, 2001 (1972).

[11] E. Yablonovitch and J. Goldhar, Appl. Phys. Lett. 25, 580 (1974).

[12] H. S. Kwok and Eli Yablonovitch, Rev. Sci. Instr. 46, 814 (1975).

[13] O. R. Wood, Proc. of IEEE, 62, 355 (1974).

[14] E. Fill, K. Hohla, G. T. Schappert and R. Volk, Appl. Phys. Lett. 29, 805 (1976).

[15] H. S. Kwok and Eli Yablonovitch, Opt. Comm. to be published.

[16] Yu, P. Raizer, Sov. Phys. JETP, 21, 1009 (1965).

[17] Eli Yablonovitch, Phys. Fluids, to be published.

[18] Eli Yablonovitch, Phys. Rev. Lett. 35, 1346 (1975).

[19] S. I. Anisimov, M. F. Ivanov, P. P. Pashinin and A. M. Prokhorov, JETP Letters 22, 161 (1975).

[20] P. K. Kaw, J. Dawson, W. Kruer, C. Oberman and E. Valeo, Kvantovaya Elektron (Moscow) 1, 3 (1971). [Sov. J. Quant. Elec. 1, 205 (1975)]

[21] J. P. Friedberg, R. W. Mitchell, R. C. Morse and L. I. Rudsinski, Phys. Rev. Lett. 28, 795 (1972).

[22] K. G. Estabrook, E. J. Valeo and W. C. Kruer, Phys. Fluids 18, 1151 (1975).

[23] J. M. Dawson, Phys. Rev. 113, 382 (1959).

[24] J. Albritton and P. Koch, Phys. Fluids 18, 1136 (1975).

[25] V. L. Ginzburg, The Propagation of Electromagnetic Waves in Plasmas, (Pergamon, Oxford, 1970), 2nd ed., see esp. Section 20.

[26] E. Segré, Nuclei and Particles (Benjamin, New York, 1965).

---

*Presented at the Fourth Workshop on "Laser Interaction and Related Plasma Phenomena" held at RPI, Troy, New York, November 8-12, 1976.